Received: 28 August 2017 | Revised: 20 September 2017 | Accepted: 21 September 2017

DOI: 10.1111/pce.13083

WILEY Plant, Cell & Environment

ORIGINAL ARTICLE

Phenomics allows identification of genomic regions affecting maize stomatal conductance with conditional effects of water deficit and evaporative demand

Santiago Alvarez Prado | Llorenç Cabrera-Bosquet | Antonin Grau | Aude Coupel-Ledru | Emilie J. Millet | Claude Welcker | François Tardieu

LEPSE, INRA, Univ. Montpellier, 34060 Montpellier, France

Correspondence
François Tardieu, INRA, Laboratoire d'Ecophysiologie des Plantes sous Stress Environnementaux, UMR759, 34060 Montpellier, France.
Email: francois.tardieu@inra.fr

Funding information
Seventh Framework Programme, Grant/Award Number: FP7-609398 and FP7-KBBE-244374; European Union's Seventh Framework Program, Grant/Award Number: FP7-609398; Agence Nationale de la Recherche, Grant/Award Number: ANR-10-BTBR-01 and ANR-11-INBS-0012; European project, Grant/Award Number: FP7-244374

Abstract

Stomatal conductance is central for the trades-off between hydraulics and photosynthesis. We aimed at deciphering its genetic control and that of its responses to evaporative demand and water deficit, a nearly impossible task with gas exchanges measurements. Whole-plant stomatal conductance was estimated via inversion of the Penman–Monteith equation from data of transpiration and plant architecture collected in a phenotyping platform. We have analysed jointly 4 experiments with contrasting environmental conditions imposed to a panel of 254 maize hybrids. Estimated whole-plant stomatal conductance closely correlated with gas-exchange measurements and biomass accumulation rate. Sixteen robust quantitative trait loci (QTLs) were identified by genome wide association studies and co-located with QTLs of transpiration and biomass. Light, vapour pressure deficit, or soil water potential largely accounted for the differences in allelic effects between experiments, thereby providing strong hypotheses for mechanisms of stomatal control and a way to select relevant candidate genes among the 1–19 genes harboured by QTLs. The combination of allelic effects, as affected by environmental conditions, accounted for the variability of stomatal conductance across a range of hybrids and environmental conditions. This approach may therefore contribute to genetic analysis and prediction of stomatal control in diverse environments.

KEYWORDS

drought, evaporative demand, GWAS, maize (*Zea mays* L.), phenomics, QTL by environment interaction, stomatal conductance, transpiration

1 | INTRODUCTION

The genetic and environmental controls of stomatal conductance are essential for the maintenance of leaf water potential at values compatible with plant metabolism and for the trade-off between photosynthesis and transpiration (Blatt, 2000; Buckley, 2005). Stomatal conductance is usually estimated via gas-exchange measurements at single-leaf level, most often under controlled light and vapour pressure deficit (VPD). Because this method is time-consuming, it is hardly compatible with the analysis of hundreds of genotypes required for precise genetic dissections (Koester, Nohl, Diers, & Ainsworth, 2016; Stinziano et al., 2017). Furthermore, even if environmental conditions are maintained stable in the gas-exchange chamber during measurements, the light and VPD sensed by plants before measurements largely affect stomatal conductance (Lawson & Blatt, 2014). Measurements of stomatal conductance in naturally fluctuating conditions are therefore most often associated with low reproducibility and consequently low heritability (Vialet-Chabrand et al., 2017). Measurements in stable conditions allow better reproducibility but do not take into account the time courses of stomatal closure and opening in response to rapid changes in light (*e.g.*, shading by a cloud; Lawson, Kramer, & Raines, 2012). Integrated over weeks, this might generate large differences in overall conductance between genotypes presenting different kinetics of responses, not observable in stable conditions (Lawson et al., 2012).

The genetic variability of stomatal control has been indirectly evaluated via the response of transpiration to VPD (Sinclair, Hammer, &

van Oosterom, 2005). Genotypic variability was observed in the parameters of this response (Sadok & Sinclair, 2009; Yang et al., 2012). A difficulty arises from the fact that VPD is only one of the determinants of evaporative demand, among others. The response of transpiration to VPD can thus only be established under stable light, most often in controlled conditions (Gholipoor, Choudhary, Sinclair, Messina, & Cooper, 2013; Shekoofa, Sinclair, Messina, & Cooper, 2016; Yang et al., 2012), ensuring full stomatal opening. This can be extended to climates in which light intensity is high and stable between successive days, provided that measurements are carried out during a well-defined time window (Kholová et al., 2010; Kholová et al., 2016). In contrast, it does not apply to the genetic analysis of stomatal control in most common situations in which light and VPD fluctuate simultaneously.

The emergence of phenotyping platforms provides a novel way to avoid the methodological difficulties raised above (Tardieu, Cabrera-Bosquet, Pridmore, & Bennett, 2017). Transpiration rate of thousands of plants can be measured with a time resolution ranging from a few minutes to a few hours, thereby allowing one to establish direct relationships between changes in transpiration rate with those of light and VPD. However, the spatial variability of light received by neighbouring plants causes a major difficulty for the establishment of these relationships (Brien, Berger, Rabie, & Tester, 2013; Kozai & Kimura, 1977; Stanhill, Fuchs, Bakker, & Moreshet, 1973), together with the larger proportion of diffuse versus direct light compared to natural conditions (Poorter et al., 2016). A method has recently been developed to solve these difficulties through the evaluation of the amount of direct and diffuse light received by each individual plant of the greenhouse, obtained by combining imaging with modelling (Cabrera-Bosquet et al., 2016). Phenotyping platforms also allow precise estimation of transpiration rate, plant leaf area, and architecture of thousands of plants every day, together with soil water potential and VPD sensed by the same plants (Cabrera-Bosquet et al., 2016). Collectively, these data potentially allow one to carry out indirect estimations of stomatal conductance of thousands of plants by inversion of the Penman–Monteith equation and to analyse the response of transpiration rate to both light and VPD in hundreds of genotypes, provided that a sufficient range of variation exists for environmental conditions within the experimental datasets.

The objective of this work was to develop a non-invasive, automatized, and accurate procedure to estimate stomatal conductance in a high-throughput phenotyping platform and to perform a proof of concept of this method via a genome wide association study (GWAS) of stomatal conductance and of its response to fluctuating light and VPD. To our knowledge, we present here the first genetic dissection of stomatal conductance and of its responses to environmental conditions via an analysis of the effects of light, VPD, and soil water potential at quantitative trait locus (QTL) effect level.

2 | MATERIALS AND METHODS

2.1 | Plant material and experiments

A diversity panel of maize hybrids was generated by crossing a common flint parent (UH007) with 254 dent lines with a restricted flowering window (Millet et al., 2016). Lines were genotyped using 50 K Infinium HD Illumina array (Ganal et al., 2011), a 600 K Axiom Affymetrix array (Unterseer et al., 2014), and a set of 500 K markers obtained by genotyping by sequencing (Sandra Negro, Stéphane Nicolas and Alain Charcosset, personal communication). After quality control, 758,863 polymorphic single-nucleotide polymorphisms (SNPs) were retained for GWAS analyses.

Four experiments were carried out in the phenotyping platform PhenoArch (https://www6.montpellier.inra.fr/lepse_eng/M3P/PHENOARCH-platform; Cabrera-Bosquet et al., 2016) hosted at the M3P, Montpellier Plant Phenotyping Platforms (https://www6.montpellier.inra.fr/lepse/M3P). Sowing dates were May 14, 2012 (Spring 2012), January 21, 2013 (Winter 2013), May 13, 2013 (Spring 2013), and May 10, 2016 (Spring 2016). In all experiments, plants were grown in 9 L pots (0.19 m diameter, 0.4 m high) filled with a 30:70 (v/v) mixture of a clay and organic compost. Three seeds per pot were sown at 0.025 m depth and thinned to one per pot when leaf three emerged.

In each experiment, two levels of soil water content were imposed, namely retention capacity (well-watered, soil water potential of −0.05 MPa) and water deficit (soil water potential from −0.3 to −0.6 MPa depending on the experiment). The weight of water in each pot was calculated at the beginning of the experiment from the weight of soil and measured soil water content. Soil water content in pots was maintained at target values by watering each pot three times per day, using watering stations made up of weighting terminals with 1 g accuracy (ST-Ex, Bizerba, Balingen, Germany) and high-precision pump-watering stations (520 U, Watson Marlow, Wilmington, MA, USA). This technique allowed high reproducibility of soil water potential between genotypes presenting contrasting leaf areas. Each hybrid was replicated: three times for the well-watered and water deficit treatments in Winter 2013, Spring 2013, and Spring 2016; and 4 and two times in Spring 2012 for the well-watered and water deficit treatments, respectively.

Air temperature and humidity were measured at six positions in the platform every 15 min (HMP45C, Vaisala Oy, Helsinki, Finland). Daily incident photosynthetic photon flux density (PPFD) over each plant within the platform was estimated by combining a 2D map of light transmission, and the outside PPFD measured every minute and averaged every 15 min with a sensor placed on the greenhouse roof (SKS 1110, Skye Instruments, Powys, UK). The greenhouse temperature was maintained at 26 ± 3 °C during the day and 18 ± 1 °C during the night. Supplemental light was provided either during daytime when external solar radiation was below 300 W m^{-2} or to extend the photoperiod by using 400 W HPS Plantastar lamps (OSRAM, Munich, Germany) with 0.4 lamps m^{-2}. The amount of light supplied by lamps was taken into account in the calculations of local PPFD (Cabrera-Bosquet et al., 2016).

2.2 | Image acquisition and analysis

Red-green-blue (2056 × 2454) images taken from 13 views (12 side views from 30° rotational difference and one top view) were captured daily for each plant during the night. Top and side cameras were calibrated using reference objects in order to convert pixels into mm^2. Plant pixels from each image were segmented from those of the background and used for estimating the whole plant leaf area

and fresh biomass as described in Brichet et al. (2017). Calibration curves were constructed using multiple linear regression models based on processed images taken in 13 directions against measurements of leaf area and fresh biomass at harvest.

The time courses of leaf area and plant fresh biomass were then fitted individually to a Gompertz equation,

$$y = a \times e^{-e^{(b-cx)}} \quad (1)$$

using appropriate R scripts (R Core Team, 2014). Time courses were expressed as a function of thermal time in equivalent days at 20 °C ($d_{20°C}$, Parent, Turc, Gibon, Stitt, & Tardieu, 2010). Leaf area and fresh biomass were therefore estimated at specific times by interpolation between nonsynchronous measurement points.

2.3 | Estimation of evaporative demand in the greenhouse

The transpiration rate of the reference hybrid (B73 × UH007) was first calculated every 15 min from changes in pot weight corrected for the effect of changes in plant fresh weight and of soil evaporation estimated from the changes in the weight of pots carrying no plant. Transpiration rate per unit leaf area was then calculated by dividing transpiration by the leaf area estimated in the same plants on the same days. Then, we parametrized the Penman–Monteith equation for mimicking the transpiration of the reference hybrid,

$$ET_{ref} = \frac{s \times R_n + \rho \times C_p \times g_a \times VPD}{\lambda \times \left(s + \gamma \times \left(1 + \frac{g_a}{g_s}\right)\right)} \quad (2)$$

Inputs were net radiation (R_n) estimated for each individual plant position in the greenhouse (Cabrera-Bosquet et al., 2016) and a mean VPD measured in eight locations of the greenhouse. Because ET_{ref} refers to the maximum transpiration rate for the considered environmental conditions, g_s in Equation 2 was the maximum value reported for maize (Tardieu & Simonneau, 1998). Temperature-dependent coefficients (ρ, kg m^{-3}; γ, Pa K^{-1}; λ, J kg^{-1} and s, Pa K^{-1}) took into account mean air temperature at each time step (Jones, 1992). Because of the complex nature of air circulation within a greenhouse, which would make any calculation of aerodynamic conductance (g_a) risky and unprecise, we have calibrated it based on measured transpiration of the reference hybrid in each experiment.

2.4 | Calculation of transpiration of individual plants

The individual pot weight was recorded four times per day, before and after each irrigation. The amount of water used by each plant was estimated as

$$Water\ use\ (litres\ H_2O) = \sum (PWA\ time_i - PWB\ time_{i+1}) \quad (3)$$

where $PWA\ time_i$ is the pot weight (g) after irrigation at time i, and $PWB\ time_{i+1}$ is the pot weight (g) before irrigation at time $i + 1$.

Evapotranspiration was estimated as the difference between pots weights measured four times per day (three during day-time irrigation and one after night-time imaging). Direct soil evaporation was calculated in pots carrying plastic plants. Plant transpiration was calculated by subtracting the evaporation from evapotranspiration of each pot, after correction for plant biomass. Transpiration rate was estimated as

$$TR\ (mg\ H_2O\ m^{-2} s^{-1}) = \frac{(PWA\ time_i - PWB\ time_{i+1}) - (EPWA\ time_i - EPWB\ time_{i+1})}{LA_{i+1} \times time_{(i+1)-i}} \quad (4)$$

where $PWA\ time_i$ is the pot weight (mg) after irrigation at time i, minus plant weight at time i, $PWB\ time_{i+1}$ is the pot weight (mg) before irrigation at time $i + 1$, minus plant weight at time $i + 1$, $EPWA\ time_i$ is the weight (mg) of pot without plant after irrigation at time i, $EPWB\ time_{i+1}$ is the weight (mg) of the pot without plant before irrigation at time $i + 1$, LA_{i+1} is the leaf area (m^2) of the plant estimated through image analysis at time $i + 1$ and $time_{(i+1)-i}$ is the time (s) between two subsequent pot weights.

For each hybrid under each watering treatment, data from four experiments were combined, and a linear regression was used to describe the response of the transpiration rate to ET_{ref}. Given the linear regression, a segmented model was used to estimate a broken-line relationship using the "segmented" package in R (R Core Team, 2014). Selection of the best model was based on Davies test (Davies, 2002). For those genotypes showing a linear response, we considered the maximum ET_{ref} as the breakpoint for genetic analysis.

2.5 | Whole-plant calculation of stomatal conductance and gas-exchange measurements

An integrated stomatal conductance was estimated by inversion of the Penman–Monteith equation, from values of transpiration rate (mg H_2O m^{-2} s^{-1}), net radiation (R_n, W m^{-2}), VPD (kPa), and the optimized value of aerodynamic conductance for each experiment, as presented in Equation 2 (g_a m s^{-1}).

$$g_s = \frac{g_a TR\ \lambda\ \gamma}{s\ Rn + \rho\ C_p g_a\ VPD - TR\ \lambda\ (s + \gamma)} \quad (5)$$

This calculation was performed over 4 time-periods per day for 20 days, totalizing 40 to 80 periods for each of the 1,680 plants of the greenhouse in each of the four studied experiments (a total of 200 to 320 periods per genotype). Maximum stomatal conductance (g_{smax}) was estimated for each genotype in each experiment × scenario combination and for each scenario by combining all experiments. In those experiments conducted in spring (high light levels) where the response of stomatal conductance to PPFD was usually saturated, the mean g_s beyond 700 μmol m^{-2} s^{-1} was considered as g_{smax}. Otherwise, in those experiments with low incident light and consequently without saturating response, g_{smax} was considered by averaging g_s values beyond 400 μmol m^{-2} s^{-1}.

A portable open gas-exchange system (Li-Cor 6400XT; Li-Cor Inc., Lincoln, NE, USA) was used to measure gas-exchange of the youngest fully expanded leaf blade in 13 of the 254 hybrids of the panel, selected for their contrasting transpiration rates in previous experiments. The stomatal conductance of these leaves was measured inside the glasshouse in Exp. Spr16 from 10:00 to 14:00 hr (solar time) at 1,500 μmol photons m^{-2} s^{-1} of PPFD, a leaf temperature of 28 °C, a leaf-to-air vapour pressure deficit of approximately 1.2–1.5 kPa, and

an ambient CO_2 of 400 μmol mol^{-1}. Stomatal conductance was also measured in situ on nonshaded leaves of the canopy receiving direct light, by using a porometer (Delta T AP4; Delta-T Devices Ltd, Cambridge, UK).

2.6 | Genetic analysis

Genotypic means were calculated for each hybrid using a mixed model containing fixed hybrid effects, random replicate, and spatial effects and spatially correlated errors fitted with ASReml-R (Butler, Cullis, Gilmour, & Gogel, 2009). The spatial model was a first order autoregressive model for both rows and columns (Gilmour, Cullis, & Verbyla, 1997). Individual mixed models were fitted in each experiment by treatment combination:

$$Y = G + \underline{Row} + \underline{Col} + \underline{Rep} + \underline{E} \quad (6)$$

where *Y* is the vector of phenotypic observations, *G* the fixed genotypic effect, *Row* the random row effect, *Col* the random column effect, *Rep* the random replicate effect, and *E* the residual error variance with an AR1(*Row*):AR1(*Col*) correlation structure. The best linear unbiased estimations of the genotypic means were then used for GWAS. The same model, but with random genotypic effects, was used to estimate heritability. Generalized heritability interpreted as broad-sense mean-line heritability was estimated as

$$H^2 = 1 - \frac{PEV}{2\sigma^2 G} \quad (7)$$

where *PEV* is the mean pairwise prediction error variance of differences between genotypes, and σ^2_G is the variance component associated with genotypic effects (Cullis, Smith, & Coombes, 2006).

GWAS was performed on individual traits for each experiment by treatment combination using the procedure presented in Millet et al. (2016). Briefly, we used the single locus mixed model

$$Y = \mu + X\beta + G + E \quad (8)$$

where *Y* is the vector of phenotypic values, μ the overall mean, *X* is the vector of SNP scores, β is the additive effect, and *G* and *E* represent random polygenic and residual effects. As in Rincent et al. (2014), the variance–covariance matrix of *G* was determined by a genetic relatedness (or kinship) matrix, derived from all SNPs except those on the chromosome containing the SNP being tested. The SNP effects β were estimated by generalized least squares, and their significance (H_0: β = 0) tested with an F-statistic. Analyses were performed with FaST-LMM v2.07 (Lippert et al., 2011).

An initial set of SNPs was selected on the basis of the results of single locus GWAS by including all SNPs with $-\log_{10}$ (*p* value) larger than 5. Physical positions of significant SNPs were projected on the consensus genetic map for Dent genetic material (Giraud et al., 2014). Candidate SNPs distant less than 0.1 cM were considered as belonging to a common QTL, described via the most significant SNP in the QTL and the interval between all SNPs belonging to the QTL. Co-locations between QTLs were checked by comparing QTLs intervals (defined by all SNPs contained in the QTL) and checking for overlap.

2.7 | Dissection of *G* × *E* and QTL × *E* for g_{smax}

To investigate the structure of *G* × *E*, we first fitted a multisituation mixed model with random effects for genotype (*G*), genotype by season interaction (*G* × *S*), genotype by water treatment interaction (*G* × *T*), and experiment specific residual error variance (*E*).

$$Y = Env + PC + PC{\times}Env + \underline{G} + \underline{G{\times}S} + \underline{G{\times}T} + \underline{E} \quad (9)$$

where *Y* is the vector of all phenotypic observations, *Env* represents fixed situation-specific means, and *PC* denotes a fixed term that refers to the first 10 principal components of the kinship matrix used to correct for population structure (Millet et al., 2016) and *PC* × *Env* the situation by *PC* interaction.

The variance components of random terms were extracted following the procedure presented in Millet et al. (2016), and the standard deviations were expressed as a percentage of the general phenotypic mean. Any effect in the model can contribute to differences in phenotype for individual genotypes within a range of ± twice the standard deviation. This range was also expressed as a percentage of the general mean.

Then for investigating the structure of the QTL × *E* effects, we fitted a multienvironment model with multiple QTLs,

$$Y = Env + PC + PC{\times}Env + \textstyle\sum_{q\in Q} QTL_q^{Env} + \underline{G} + \underline{G{\times}S} + \underline{G{\times}T} + \underline{E} \quad (10)$$

with $QTL_q^{Env} = QTL_q + (QTL{\times}Env)_q$. We have fitted environment-specific QTL effects that are the sum of a QTL main effect and a QTL by environment interaction term. The set of QTL used in the model was determined by a backward elimination process over the complete set of QTLs. To assess the amount of genetic (co)variance explained by the QTLs, we compared the estimated variance components in Equation 9 with those obtained in Equation 10.

Allelic effects of all candidate QTLs were extracted from Equation 10. When no indication is provided, a positive effect indicates that the reference hybrid allele increased the trait value, whereas a negative effect indicates that the alternative allele increased the trait value.

Finally, a model considering QTL main effects, the environmental variables PPFD, VPD and soil water potential and their interaction with QTLs was used to predict g_{smax}

$$g_{smax} = \mu + PPFD + VPD + SWP + PPFD{\times}VPD + PPFD{\times}SWP + VPD{\times}SWP + \textstyle\sum_{q\in Q} QTL_q^{EnV} + \underline{E} \quad (11)$$

where μ is the phenotypic mean, *PPFD*,*VPD*,*SWP* the environmental variables, and $QTL_q^{Env} = QTL_q + (QTL{\times}Env)_q$. We have fitted environment-specific QTL effects that are the sum of a QTL main effect and a QTL by environmental variable interaction. For each of the QTLs, the part due to $(QTL{\times}Env)_q$ was dissected in the interaction of QTLs with environmental variables PPFD, VPD, and soil water potential:

$$(QTL{\times}Env)_q = (QTL_q{\times}PPFD) + (QTL_q{\times}VPD) + (QTL_q{\times}SWP) \quad (12)$$

2.8 | Candidate genes

Each QTL of g_{smax} was queried in the maize 5b annotation file ZmB73_5b_FGS_info.txt downloaded from maizesequence.org using a custom Perl script. Gene products were sought at the National Center for Biotechnology Information database (www.ncbi.nlm.nih.gov; verified April 3, 2017).

3 | RESULTS

3.1 | A large variability of growth and transpiration rate over a range of environmental conditions, with marked genotypic differences

Four datasets corresponding to experiments carried out at different times of the year were combined to generate a large range of environmental conditions, with mean values of incident light from 2.8 to 7.7 MJ m^{-2} d^{-1} (Table 1), a day-to-day coefficient of variation (CV) of VPD from 22% to 40% depending on experiments and soil water potentials ranging from −0.03 to −0.55 MPa, obtained via controlled irrigation (Table 1). This translated into large phenotypic differences across experiments. Leaf area ranged from 0.26 to 0.41 m^2 pl^{-1} (Figure 1a,b), total water use from 1.9 to 4.5 l pl^{-1} (Figure S1), and fresh biomass from 193 to 330 g pl^{-1} (Figure S1). The genotypic variability in the diversity panel was high for fresh biomass and leaf area, with variabilities of 47% and 52%, respectively, at early phenological stages (24 $d_{20°C}$ after sowing), and 46% and 47% at late stages (45 $d_{20°C}$ after sowing; Figure 1a, S1a). Broad sense heritability ranged from 0.53 to 0.78 across experiments for fresh biomass and from 0.53 to 0.83 for leaf area (Table S1). A GWAS analysis resulted in multiple QTLs presented in Table S2.

A reference evapotranspiration (ET_{ref}) was calculated on the basis of changes in pot weight of the reference hybrid, B73 × UH007, recorded every 15 min in all experiments (inset Figure 2), corrected for the effect of plant fresh weight and of soil evaporation, and divided by the leaf area estimated in the same plants on the same days. We have then parametrized the Penman–Monteith equation for mimicking the transpiration of reference hybrid. The resulting ET_{ref} closely followed this transpiration (Figure 2) and ranged from 8 to 19 mg H_2O m^{-2} s^{-1} (Figure 1c). The transpiration of individual hybrids showed a large genotypic variability (58% over the whole set of experiments, Figure 1b), with a broad sense heritability of 0.58 (Table S1). It was related to ET_{ref} with a slope that largely varied between hybrids (Figure S2 $p < .001$), indicating genotypic differences in stomatal control.

Overall, this dataset was therefore an interesting case study for testing our method of estimation of stomatal conductance and for assessing the genotypic variability of stomatal conductance and of its responses to environmental conditions.

3.2 | High-throughput calculation of stomatal conductance at whole-plant level

Stomatal conductance was calculated for each plant by inversion of the Penman–Monteith equation (Equation 5), taking into account measured values of transpiration rate, net radiation, VPD, and leaf area. This whole-plant stomatal conductance increased with PPFD, with a larger scatter of points compared with that obtained by using a gas-exchange equipment with controlled light on a single leaf (Figure 3a,b). However, this scatter took into account different plants of the same hybrid on different days and was similar to that of measurements performed on different plants and days with the gas-exchange device (not shown). Furthermore, g_s at the whole-plant level showed a lower plant-to-plant variability than in situ values at leaf level measured with a porometer on plants receiving natural light (Figure S3). As expected, g_s at the whole-plant level was lower than that at leaf level because the whole-plant g_s integrated the whole leaf area with only part of it receiving full light (inset Figure 3b).

Maximum stomatal conductance (g_{smax}) was estimated for each hybrid in each combination experiment × scenario, as the mean g_s at PPFD beyond 700 µmol m^{-2} s^{-1}, or beyond 400 µmol m^{-2} s^{-1} in the winter experiment with low incident light. Mean values corresponding to each hybrid closely correlated with those measured with a gas exchange device in well-watered conditions but with lower values (R^2 = 0.54, Figure 4a). The difference in g_{smax} between well-watered and water deficit conditions was also accounted for by our method (overall R^2 = 0.85, CV of error of 13%). In water deficit, the genotypic variability of g_{smax} did not match between single-leaf and whole-plant measurements, possibly because of different distributions of stomatal closure between leaves in the tested hybrids. The estimated g_{smax} was also positively associated with biomass accumulation per unit leaf area over the whole panel (Figure 4b, overall R^2 = 0.58). This relationship probably reflected the control that stomatal conductance exerts over cumulated photosynthesis through the regulation of transpiration rate (Fig. S4; R^2 = 0.66, CV = 7.5%). Overall, these results suggest that the method presented here can be used as a surrogate of gas-exchange for analysing the genetic variability of stomatal conductance.

TABLE 1 Environmental variables and watering scenarios of the four experiments. Data are averaged for a period running from 24 $d_{20°C}$ (eight visible leaves) to 45 $d_{20°C}$ (14 visible leaves)

Season	Year	ID	T_{max} (°C)	T_{min} (°C)	T_{mean} (°C)	VPD_{max} (kPa)	VPD_{min} (kPa)	VPD_{mean} (kPa)	$Light_{mean}$ (MJm^{-2})	Scenario WW (MPa)	WD (MPa)
Spring	2012	Spr12	32.8	20.7	25.1	2.9	0.6	1.3	5.9	−0.09	−0.45
Winter	2013	Win13	29	19.5	21.3	2.4	0.9	1.4	3.2	−0.09	−0.35
Spring	2013	Spr13	32	17.1	23.4	2.6	0.6	1.1	6	−0.08	−0.3
Spring	2016	Spr16	31.4	16	23.5	1.9	0.3	1.0	7.7	−0.03	−0.55

Note. VPD = vapor pressure deficit; WW = well-watered; WD = water deficit.

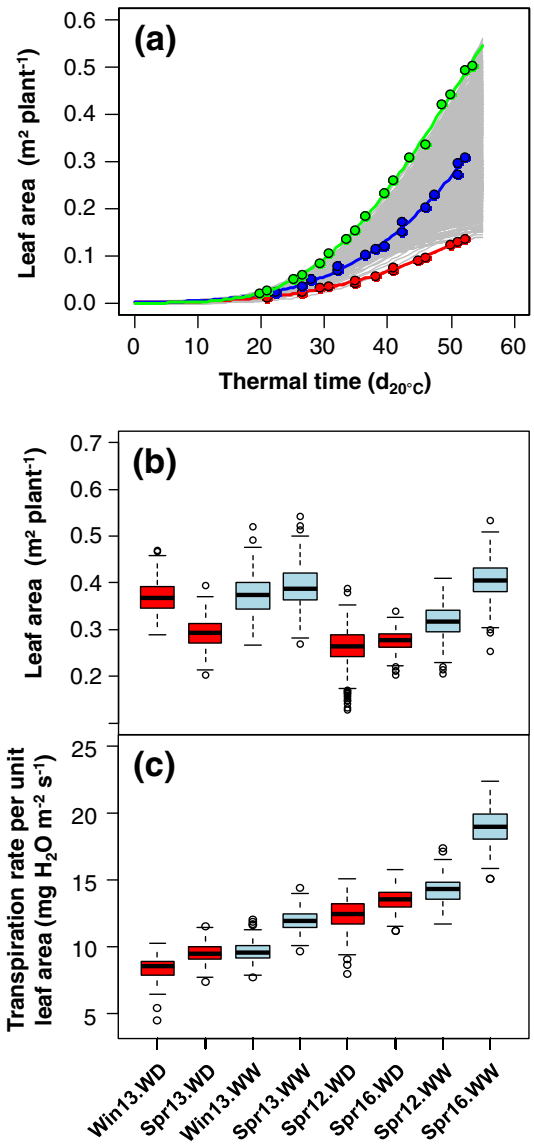

FIGURE 1 Genotypic and environmental variabilities of leaf area and transpiration rate in the studied dataset. (a) Change with time of leaf area for the 254 hybrids of the panel during one experiment (Exp. Spr12). (b) Leaf area at 45 $d_{20°C}$ after sowing in the eight situations. (c) Mean transpiration rate per unit leaf area from 24 to 45 $d_{20°C}$. In (a), green, blue, and red lines represent plants of the hybrids with maximum, median, and minimum growth rate, respectively. Grey lines represent the rest of the panel. Each point represents one measurement. In (b) and (c), boxes and vertical bars represent the genotypic variability in well-watered (light blue) and water deficit (red) situations. Horizontal bars, median, boxes, and vertical bars represent 5%, 25%, 50%, 75% and 95% quantiles [Colour figure can be viewed at wileyonlinelibrary.com]

3.3 | Genetic analysis of g_{smax} revealed QTLs whose allelic effects responded to VPD, light, or soil water potential

A large genotypic variability was observed for g_{smax} in each experiment (as illustrated for one experiment in Figure 5), with a genotypic variation (*G*) affecting the mean g_{smax} by ±8.6% (Table 2). The genotype by environment interaction affected g_{smax} by ±3.8% for watering treatments (*G* × *T*) and ±4.4% for seasons (*G* × *S*; Table 2, Figure S5). The broad sense heritability of g_{smax} was 0.57 and 0.56 under well-watered and water deficit, respectively, in Exp. Spr16 (Figure 5; Table S1).

A GWAS analysis was performed on g_{smax} estimated in each experiment or combining all experiments. This resulted in 29 and 20 QTLs under well-watered and water deficit conditions, respectively (Table S2). Among those, 16 QTLs were retained after using the backward elimination procedure that allows eliminating redundant QTLs. They captured 58% of the additive genetic variance of g_{smax} (Table 2) and an appreciable part of the genotype by environment interaction, namely 33% and 40% of the *G* × *T* and the *G* × *S* interactions (Table 2). Sixteen of them co-localized, within 0.1 cM, with QTLs for transpiration rate (Fig. S6; Table S2), three with QTLs of fresh biomass, and six with QTLs of leaf area (Table S2). Four co-localized with QTLs of the slope of the relationship between transpiration rate and evaporative demand (Fig. S6).

The 16 QTLs of g_{smax} harboured from 1 to 19 genes, except for QTLs on bins 2.05 and 4.05 (Table 3). Their allelic effects largely differed between experiments, opening the possibility that QTL effects may depend on the environmental conditions that affect phenotypic values of stomatal conductance. This translated into the classical result of a high QTL by environment interaction, with only two of the 16 QTLs significant in more than five experiment by water regime combinations (Table S3). We have therefore tested if the effects of light, VPD, and soil water potential on stomatal conductance translated at QTL level, thereby indicating possible mechanisms of stomatal control and providing an efficient way to select likely candidate genes among the 1–19 that were located within the QTL interval.

- Vapour pressure deficit affected the allelic effects of three QTLs (bins 2.05, 4.05, and 6.00; example on Figure 6b). Interestingly, two of them were also significantly affected by light but with opposite directions, as observed for phenotypic data. Among the genes within the QTL intervals, we identified three abscisic acid (ABA) transcription factors (myeloblastosis, N-acetyl cysteine, and basic-leucine zipper) and two ethylene related proteins (AP2-EREBP and ethylene receptor homolog 40), all of them involved in the drought-induced processes of stomatal closure (Table S4). In addition, the QTL on bin 2.05 co-localized with a QTL that constitutively affects the discrimination of stable carbon isotope ($\Delta^{13}C$), which is associated with stomatal closure under water deficit conditions (Gresset et al., 2014). QTL co-location between g_{smax} and $\Delta^{13}C$ was also observed on bins 5.02, 7.02, and 7.03.
- Light alone (independently of VPD) affected the allelic effects of three QTLs (Figure 6a,c, bins 2.05, 6.00 and 8.05), thereby accounting for part of the genotype by season interaction (Table 2). Among the five and seven genes in the confidence interval of these QTLs (except for one of them), two genes were related to stomatal response to light via biosynthesis and transport genes, namely a flavonoid ABC transporter (G family member 10) and auxin-induced protein (IAA27; Table S4). Flavonoids control the polar transport of auxin involved in stomatal control (Terasaka et al., 2005).

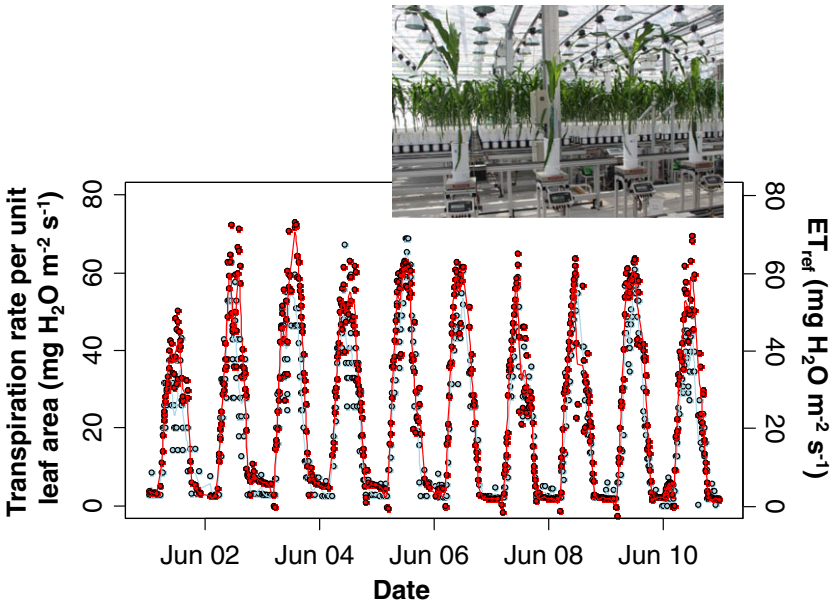

FIGURE 2 Daily time courses of transpiration rate (light blue lines and symbols) of hybrid B73 × UH007 and reference evapotranspiration (ET_{ref}, red lines and symbols) estimated via the Penman–Monteith equation (Exp. Spr16). Inset, plants of hybrid B73 × UH007 placed on balances for estimation of transpiration every 15 min. Only plants on balances are presented here for easier understanding but, during experiments, these plants are surrounded by four plants each, thereby creating a mini canopy [Colour figure can be viewed at wileyonlinelibrary.com]

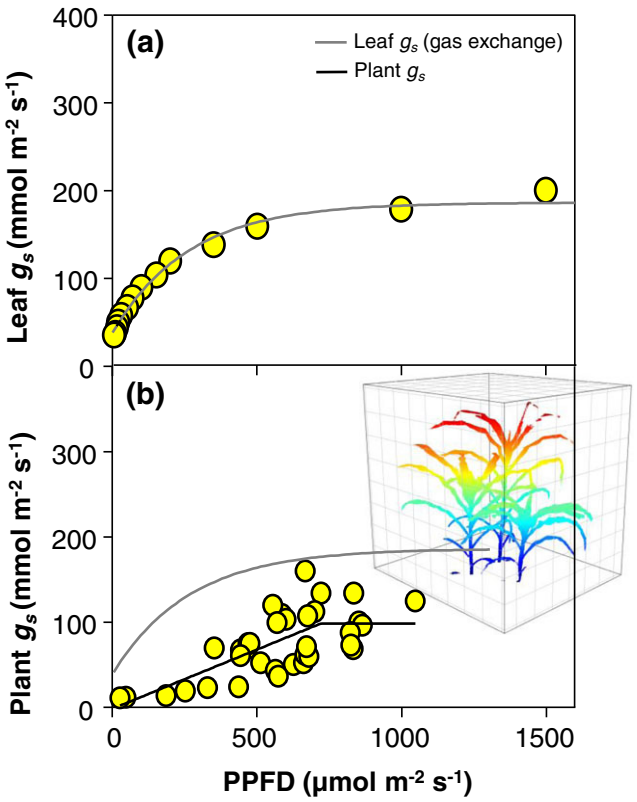

FIGURE 3 Relationship between incident light photosynthetic photon flux density (PPFD) and (a) stomatal conductance at leaf scale (leaf g_s) measured with a gas-exchange device and (b) calculated stomatal conductance at plant scale (plant g_s) estimated via inversion of the Penman–Monteith equation. In (a) and (b), the grey curve represents the fit for leaf g_s. In (b), the black curve represents the fit for plant g_s. Inset, virtual 3D plant with colours representing intercepted light for each leaf pixel. Data in (a), (b), and inset were collected on the reference hybrid B73 × UH007 [Colour figure can be viewed at wileyonlinelibrary.com]

- Soil water potential affected the allelic effect of three QTL (bin 4.01, 7.04, and 10.04; example on Figure 6d), thereby accounting for part of the genotype by treatment interaction (Table 2). Among the 3 and 15 genes in the confidence interval of the QTLs (Table 3), we have identified a protein kinase (dual specificity protein kinase shkE) involved in ABA-induced stomatal closure under water deficit (Brock et al., 2010).

Independently of their putative action, the QTLs and relationships presented above allow estimation of stomatal conductance across genotypes and environmental scenarios. For the 13 hybrids previously compared with gas-exchange measurements, observed values of g_{smax} were accounted for by values of light, VPD, and soil water potential across situations (Figure 7, R^2 = 0.77–0.97). As expected, the estimated effects were usually smaller than observed effects, resulting in slopes smaller than 1 in the observed—predicted graphs corresponding to each hybrid in Figure 7. This was due to the fact that significant QTLs detected in this analysis accounted for 58% of the genetic variability. It is nevertheless remarkable that more than half of the genetic variability of g_s was accounted for in this analysis.

4 | DISCUSSION

4.1 | Exploiting the environmental variability for analysing gas-exchange at the whole-plant level

Reproducibility of experiments in phenotyping platforms is difficult because, even if temperature is controlled, different experiments are carried out under varying vapour pressure deficit associated to changes in air dew point temperature and varying light intensity associated with time of year, cloud cover, and shading from greenhouse structure and neighbouring plants (Cabrera-Bosquet

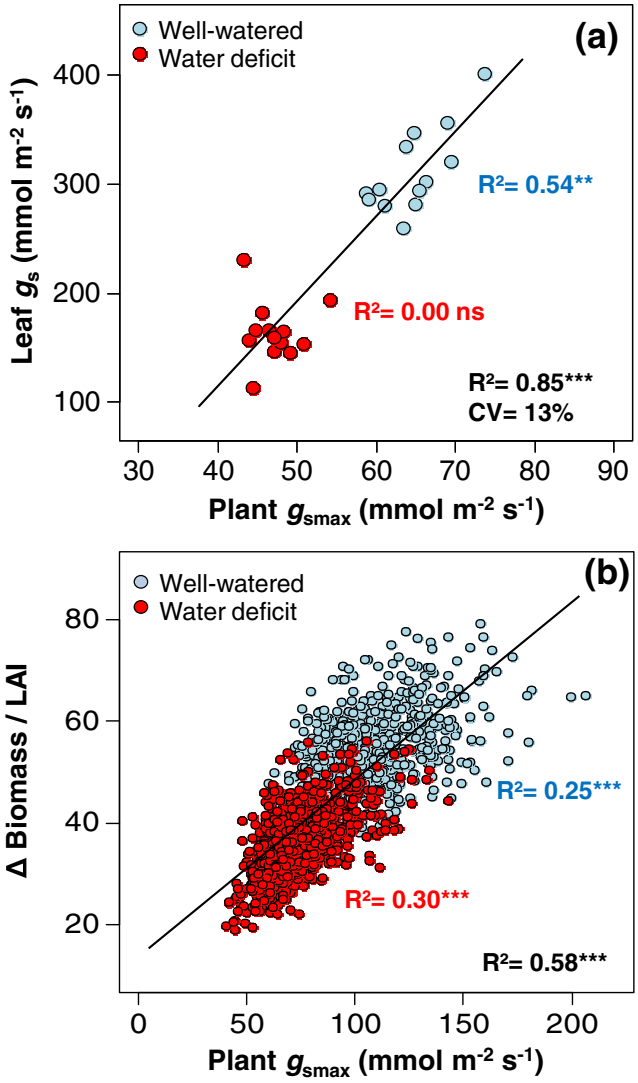

FIGURE 4 Relationship between maximum stomatal conductance estimated via inversion of the Penman–Monteith equation (g_{smax}) between leaf Stages 8 and 14, and (a) stomatal conductance measured with a gas-exchange device (leaf g_s) in 13 maize hybrids either under well-watered or water deficit conditions; (b) the ratio between accumulated fresh biomass and leaf area index of plants between leaf Stages 8 and 10 in 254 hybrids (Exp. Spr16) [Colour figure can be viewed at wileyonlinelibrary.com]

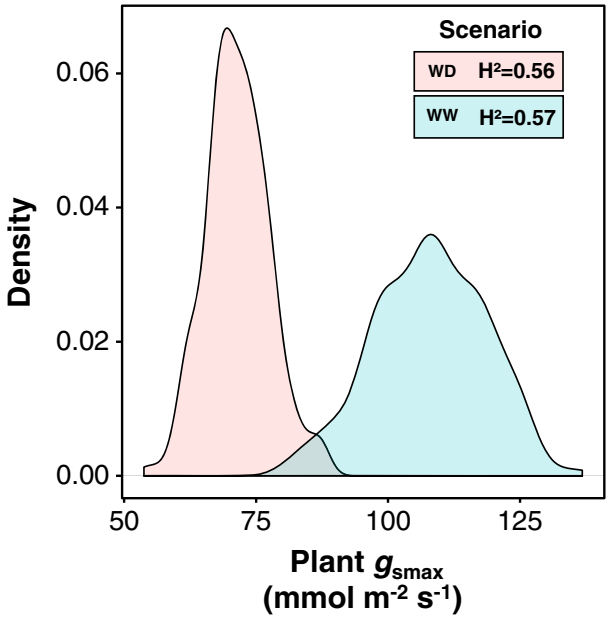

FIGURE 5 Genotypic variability and heritability of stomatal conductance estimated via inversion of the Penman–Monteith equation (g_{smax}) under water deficit (WD, red) and well-watered (WW, light blue) conditions. The *y* axis represents the probability density. Inset, heritabilities in WD and WW conditions (Exp. Spr16) [Colour figure can be viewed at wileyonlinelibrary.com]

et al., 2016; Lawson et al., 2012). This is often viewed as an argument in favor of fully controlled conditions in growth chambers. However, phenotyping in stable conditions is not a panacea in view of the importance of mechanisms during non-steady states (Baerenfaller et al., 2012; Lawson & Blatt, 2014). Here, inversion of the Penman–Monteith equation (Monteith, 1965) allowed us to exploit the variability of light and VPD along day or night cycles and seasons for estimation of stomatal conductance and of its changes with environmental conditions.

- Calibrating the Penman–Monteith equation for daily variations within each experiment has enabled us to solve the problem of estimation of aerodynamic conductance. The latter can be based on energy balance following short-term changes in temperature (Tarara & Ham, 1999), but the complex nature of air fluxes in the greenhouse, the rapid change with time of canopy architecture, and the movements of plants in the greenhouse would have led to serious inaccuracy. Instead, we have optimized this parameter to mimic changes in transpiration rate during day or night cycles with varying light and evaporative demand (Figure 2). This has allowed us to estimate a reference evaporative demand every 15 min, which considered temporal and spatial variations in both light and VPD for each plant within the platform.
- Estimating transpiration rate several times per day for each plant and combining it between experiments has allowed us to obtain integrated estimations of stomatal conductance and of its response to light and VPD. This has avoided the difficulty of rapid changes in stomatal conductance at leaf level. Indeed, gas-exchange measurements in these conditions result in a very large variability of g_s (Fig. S3) and also in frequent overestimations due to the succession of shade and sun flexes (Rochette et al., 1991).
- Considering experiments at different seasons has allowed us to, partly, disentangle the respective effects of light and VPD that are usually well correlated during a single experiment. Indeed, diurnal changes in VPD are essentially due to changes in temperature, themselves closely correlated with light. Because dew point temperature differs between seasons, higher VPD were obtained in winter whereas light was lower, thereby breaking the usual correlation between these terms. It is noteworthy that large stability of light in subtropical environments is an advantage for establishing direct relationships between VPD

TABLE 2 Variance components of the different mixed models for whole-plant stomatal conductance (g_{smax})

Statistical model	Type	G[a]	$G \times T$[b]	$G \times S$[c]	Res[d]
Model 1: Multi-envt	Variance components (mmol m^{-2} s^{-1})^2	5.9	1.2	1.5	32.9
Model 2: Multi-envt, multi locus	Variance components (mmol m^{-2} s^{-1})^2	2.5	0.8	0.9	27.7
Model 1: Multi-envt	SD as % of mean	4.3	1.9	2.2	10.2
Model 2: Multi-envt, multi locus	SD as % of mean	2.8	1.6	1.7	9.3
QTLs (diff. Var. comp. Model)		58	33	40	16

Note. The general mean of g_{smax} was 56.42 mmol m^{-2} sec^{-1}.

QTLs = quantitative trait loci; G = genotype; $G \times T$ = genotype by water treatment interaction; $G \times S$ = genotype by season interaction.

[a]Genotype.

[b]Genotype by water treatment interaction.

[c]Genotype by season interaction.

[d]Experiment-specific residual error variance.

TABLE 3 Final set of QTLs of whole-plant stomatal conductance (g_{smax}; mmol m^{-2} s^{-1}) with position, region, situation, effects, and number of genes in the region around QTL position

SNP name[a]	SNP position (pb)[b]	Bin[c]	Region (Mbp)[d]	Region (cM)[d]	Situation[e]	LogPval[f]	Allelic effect[g]	Gene #[h]
S1_5744907	5744907	1.01	5.7–5.79	12.65–12.85	Spr13.WD	5.82	1.15	3
AX-90724010	280381987	1.10	280.31–280.46	230.18–230.38	Spr12.WD	5.95	−2.21	1
PZE-102095227	108996680	2.05	84.45–132.54	94.88–95.08	Mean WW and WD	5.15	1.72	425
AX-91442117	127216610	3.05	126.64–127.78	60.42–60.62	Spr16.WW	5.14	3.02	19
AX-90856058	2435073	4.01	2.41–2.48	7.08–7.28	Spr13.WW	5.42	−1.51	3
S4_122293518	122293518	4.05	92.39–126.79	54.45–54.66	Spr12.WW	6.78	−2.86	250
S5_11921464	11921464	5.02	11.88–11.97	36.50–36.70	Spr13.WD	5.46	−1.19	6
AX-90979141	3854510	6.01	3.69–3.94	3.50–3.79	Win13.WW	5.12	1.39	5
S6_150840088	150840088	6.05	150.77–150.92	71.63–71.83	Spr12.WD	5.49	2.24	8
S6_158480562	158480562	6.06	158.45–158.52	89.80–90.01	Spr12.WW	5.53	−2.38	7
S7_124403341	124403341	7.02	124.35–124.46	55.09–55.29	Spr16.WW	5.67	3.07	2
S7_128646920	128646920	7.03	128.6–128.71	63.24–63.44	Win13.WW	5.00	−1.26	3
SYN29618	160060267	7.04	160–160.14	91.40–91.62	Win13.WW	6.70	1.47	9
AX-91435380	143564041	8.05	143.3–143.94	126.39–126.64	Spr16.WD	5.75	−1.94	7
AX-91804303	139953567	9.06	139.89–140.02	91.46–91.66	Spr12.WW	5.63	2.34	8
AX-91189633	124235924	10.04	123.96–124.52	80.07–80.27	Spr12.WW	5.19	2.22	15

Note. QTL = quantitative trait loci; SNP = single-nucleotide polymorphisms; WW = well-watered; WD = water deficit.

[a]SNP with the highest $-\log_{10}(p\text{-value})$.

[b]SNP physical position.

[c]Chromosome and bin.

[d]QTL region (in physical and genetic units).

[e]Experiment by scenario combination where the QTL was initially significant.

[f]$-\log_{10}(p\text{-value})$.

[g]Allelic effect in the specific situation.

[h]Number of genes in the QTL interval.

and transpiration (Kholová et al., 2010; Kholová et al., 2016), but the variability in temperate climate allows addressing a wider range of environmental conditions provided that several seasons are combined.

Overall, the method proposed here allowed estimation of the genetic and environmental variabilities of stomatal conductance of thousands of plants, a nearly impossible task with methods based on gas exchanges. Whole-plant conductance was well related to gas exchanges and biomass, had an appreciable heritability, and could be dissected into well-organized QTLs. This suggests that the noise associated with errors, estimates, and hypotheses at different step of the method did not hamper the usefulness of our method. The lower values of whole-plant conductance compared with gas exchanges were expected due to the large part of leaf area that is shaded in a canopy. We acknowledge that this may

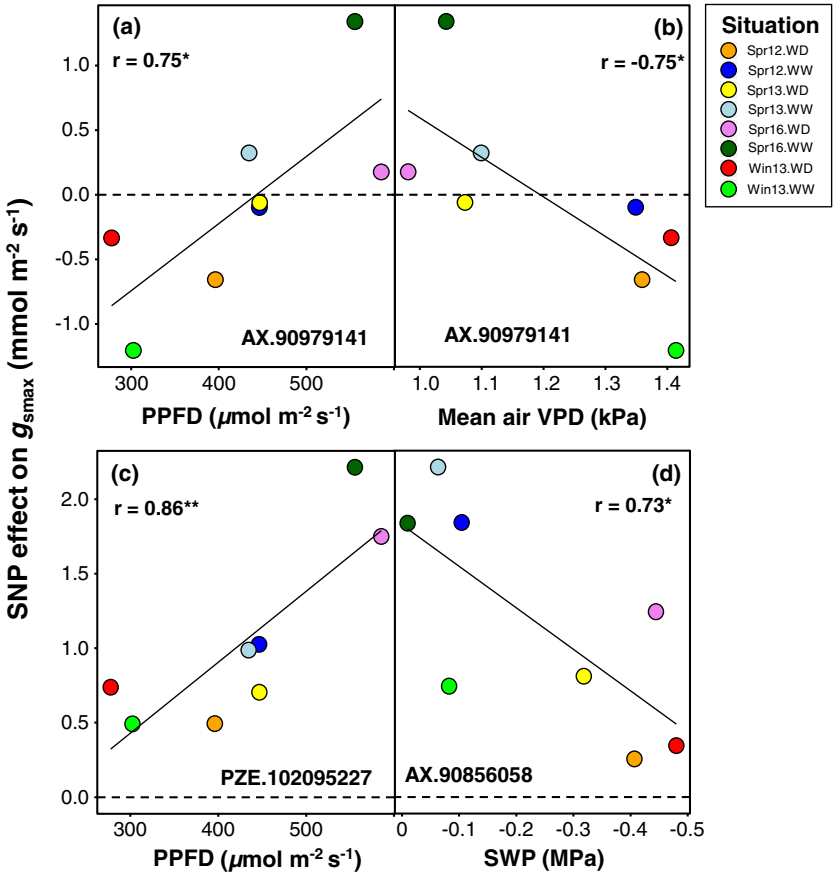

FIGURE 6 Allelic effects of quantitative trait loci (QTLs) of estimated stomatal conductance (g_{smax}) as a function of environmental variables. (a) and (b), allelic effect of QTL on chromosome 6.00 (3.85 Mb) as a function of photosynthetic photon flux density (PPFD) and vapour pressure deficit (VPD), respectively; (c), allelic effect of QTL on chromosome 8.05 (143.56 Mb) as a function of PPFD; (d), allelic effect of QTL on chromosome 4.01 (2.43 Mb) as a function of soil water potential. Each colour, one experiment. SNP = single-nucleotide polymorphisms; SWP = soil water potential [Colour figure can be viewed at wileyonlinelibrary.com]

buffer part of the genetic variability, but it also buffers temporal and spatial changes that blur integrated estimates based on gas exchanges.

4.2 | Dissecting the effects of evaporative demand on stomatal conductance through genetic analysis

The high QTL × *E* interaction for stomatal conductance resulted in QTL instability, already observed in previous studies using a gas-exchange device (Fracheboud, Ribaut, Vargas, Messmer, & Stamp, 2002). In particular, all QTLs identified here displayed a high and significant QTL × *E* interaction, similar to that for yield (Bonneau et al., 2013; Millet et al., 2016). Despite this high instability, QTLs of stomatal conductance co-localized with QTLs of transpiration rate and biomass (Table S2) and with QTLs of $\Delta^{13}C$ (Gresset et al., 2014), which is directly associated with stomatal conductance under water deficit conditions.

The differential responses of allelic effects at QTLs suggest that the well-known effect of light, soil water potential and VPD on stomatal conductance may act at gene level, in addition to whole-plant controls. (a) Two QTLs had allelic effects that responded to light and VPD in opposite ways, suggesting that opposite effects of light and VPD may act at gene level. This suggestion was supported by the presence of auxin-related genes, involved in the inhibition of ABA-induced stomatal closure through the modulation of ethylene biosynthesis (also found within the QTL intervals) that reduce osmotic pressure in the guard cells (Tanaka et al., 2006). (b) Other QTLs were responsive to VPD but not to light, suggesting a hydraulic effect, which was endorsed by a gene involved in ABA synthesis (Cominelli et al., 2005). (c) One QTL was responsive to light but not to VPD, containing a gene involved in transport and biosynthesis of the growth hormone auxin (Terasaka et al., 2005). (d) Three QTLs responded to soil water potential but not to VPD, suggesting independence of these two effects, with genes related to a protein kinase, which directly interacts with ABA-inducible genes that trigger stomatal closure (Brock et al., 2010). (e) Finally, eight QTLs had allelic effects that responded to none of the studied environmental variables, suggesting either that they were constitutive (e.g., stomatal density or shape), or that our method could not detect environmental effects on their allelic values.

When considering all QTL effects and their interactions with environmental variables in a model, the phenotypic variability due to different environmental scenarios in the four experiments was reasonably accounted for in the tested genotypes. However, about half of the genetic variability was not taken into account by significant QTLs, as commonly observed in other studies (Alvarez Prado, López, Gambín, Abertondo, & Borrás, 2013; Malosetti, Ribaut, Vargas, Crossa, & van Eeuwijk, 2008). This was probably due to the presence of small-effect QTLs that were not significant for the selected threshold. An approach based on genomic prediction, jointly taking into account the effects of hundreds of small-effect SNPs within a statistical model, would probably capture a larger proportion of the genetic variability, which was not explained here by a limited number of significant QTLs (Moser et al., 2015).

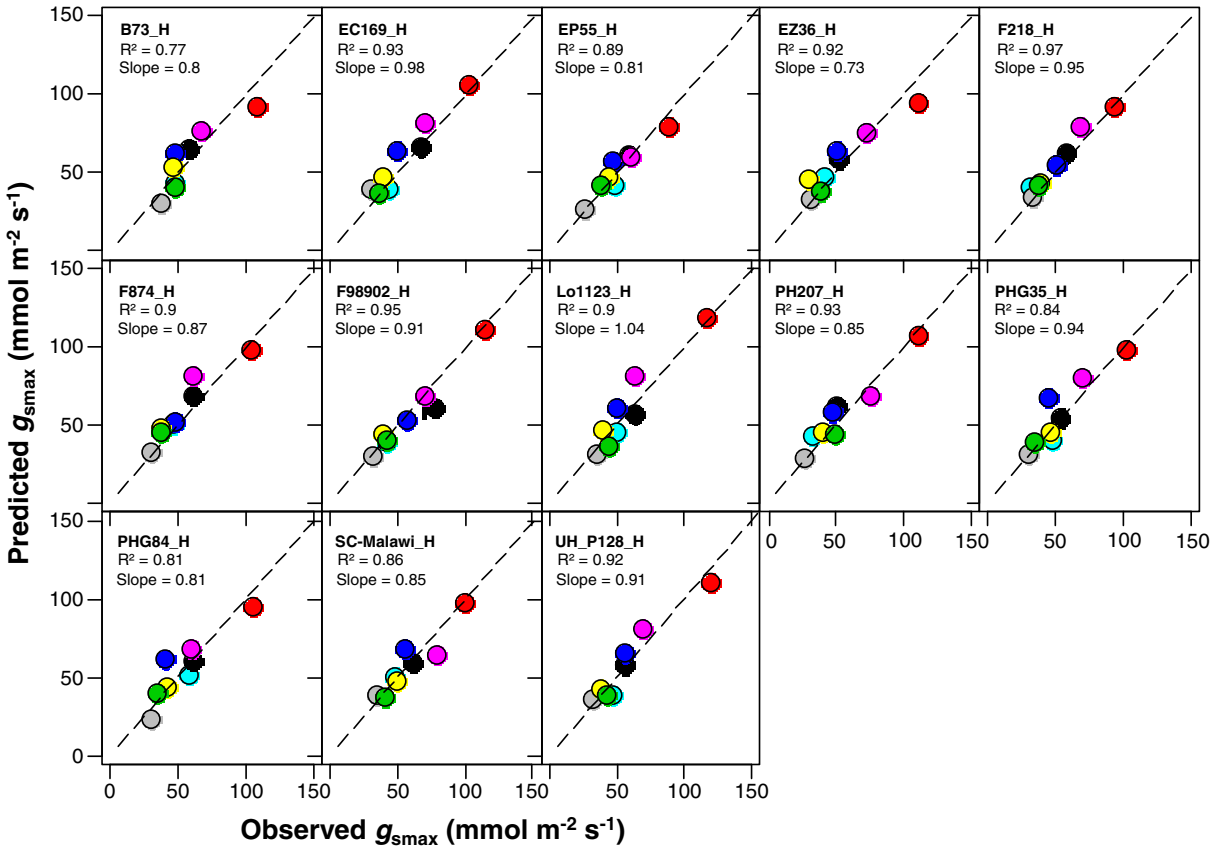

FIGURE 7 Predicted g_{smax} plotted against observed g_{smax} for the 13 selected hybrids using Equation 11. Prediction was performed by considering detected quantitative trait loci, photosynthetic photon flux density, vapour pressure deficit, and soil water potential effects and their interactions. Each colour represents one situation (experiment by scenario combination): Red, pink, blue, black, lightblue, yellow, green, and grey represent Spr16.WW, Spr16.WD, Spr13.WW, Spr13.WD, Spr12.WW, Spr12.WD, Win13.WW, and Win13.WD, respectively. R-square and the regression parameters are included for each hybrid [Colour figure can be viewed at wileyonlinelibrary.com]

Hence, we believe that the method presented here can bring new elements for analysing the genetic architecture of environmental effects on stomatal conductance.

ACKNOWLEDGMENTS

This work was supported by the European project FP7-244374 (DROPS) and the Agence Nationale de la Recherche project ANR-10-BTBR-01 (Amaizing) and ANR-11-INBS-0012 (Phenome). SAP has been funded by the European Union's Seventh Framework Program under grant agreement FP7-609398, through the award of an AgreenSkills+ fellowship. We are grateful to Benoit Suard, Pauline Sidawy, Cloé Check, Aude Pasquier, and Thomas Laisné from INRA-LEPSE for their technical assistance during the experiments. We thank Carine Palaffre (INRA St. Martin de Hinx) for seed increase. We also acknowledge Alain Charcosset, Sandra Negro, and Stéphane Nicolas from INRA Le Moulon who developed the genotyping and the pipeline for GWAS analysis. We finally thank Björn Usadel for helping with bioanalysis.

AUTHOR CONTRIBUTIONS

S. A. P. and F. T. designed the research, analysed results, and wrote the manuscript.

L. C. -B., A. G., S. A. P., and C. W. performed the experiments. E. J. M., A. C. -L., and C. W. participated to the genetic analyses.

ORCID

Santiago Alvarez Prado http://orcid.org/0000-0003-0433-5222
Llorenç Cabrera-Bosquet http://orcid.org/0000-0002-2147-2846
Aude Coupel-Ledru http://orcid.org/0000-0003-2097-5924
François Tardieu http://orcid.org/0000-0002-7287-0094

REFERENCES

Alvarez Prado, S., López, C. G., Gambín, B. L., Abertondo, V. J., & Borrás, L. (2013). Dissecting the genetic basis of physiological processes determining maize kernel weight using the IBM (B73 × Mo17) Syn4 population. *Field Crops Research*, *145*, 33–43.

Baerenfaller, K., Massonnet, C., Walsh, S., Baginsky, S., Buhlmann, P., Hennig, L., … Gruissem, W. (2012). Systems-based analysis of Arabidopsis leaf growth reveals adaptation to water deficit. *Molecular Systems Biology*, *8*, 606.

Blatt, M. R. (2000). Cellular signaling and volume control in Stomatal movements in plants. *Annual Review of Cell and Developmental Biology*, *16*, 221–241.

Bonneau, J., Taylor, J., Parent, B., Bennett, D., Reynolds, M., Feuillet, C., … Mather, D. (2013). Multi-environment analysis and improved mapping of a yield-related QTL on chromosome 3B of wheat. *Theoretical and Applied Genetics*, *126*, 747–761.

Brichet, N., Fournier, C., Turc, O., Strauss, O., Artzet, S., Pradal, C., … Cabrera-Bosquet, L. (2017). A robot-assisted imaging pipeline for tracking the growths of maize ear and silks in a high-throughput phenotyping platform. *Plant Methods* 13:96.

Brien, C. J., Berger, B., Rabie, H., & Tester, M. (2013). Accounting for variation in designing greenhouse experiments with special reference to greenhouses containing plants on conveyor systems. *Plant Methods*, *9*, 5.

Brock, A. K., Willmann, R., Kolb, D., Grefen, L., Lajunen, H. M., Bethke, G., … Gust, A. A. (2010). The Arabidopsis mitogen-activated protein kinase phosphatase PP2C5 affects seed germination, stomatal aperture, and abscisic acid-inducible gene expression. *Plant Physiology*, *153*, 1098–1111.

Buckley, T. N. (2005). The control of stomata by water balance. *New Phytologist*, *168*, 275–292.

Butler, D. G., Cullis, B. R., Gilmour, A. R., & Gogel, B. J. (2009). *ASReml-R User Guide Release*, 3.0.

Cabrera-Bosquet, L., Fournier, C., Brichet, N., Welcker, C., Suard, B., & Tardieu, F. (2016). High-throughput estimation of incident light, light interception and radiation-use efficiency of thousands of plants in a phenotyping platform. *New Phytologist*, *212*, 269–281.

Cominelli, E., Galbiati, M., Vavasseur, A., Conti, L., Sala, T., Vuylsteke, M., … Tonelli, C. (2005). A guard-cell-specific MYB transcription factor regulates Stomatal movements and plant drought tolerance. *Current Biology*, *15*, 1196–1200.

Cullis, B. R., Smith, A. B., & Coombes, N. E. (2006). On the design of early generation variety trials with correlated data. *Journal of Agricultural, Biological, and Environmental Statistics*, *11*, 381.

Davies, R. B. (2002). Hypothesis testing when a nuisance parameter is present only under the alternative: Linear model case. *Biometrika*, *89*, 484–489.

Fracheboud, Y., Ribaut, J. M., Vargas, M., Messmer, R., & Stamp, P. (2002). Identification of quantitative trait loci for cold-tolerance of photosynthesis in maize (*Zea mays* L.). *Journal of Experimental Botany*, *53*, 1967–1977.

Ganal, M. W., Durstewitz, G., Polley, A., Berard, A., Buckler, E. S., Charcosset, A., … Falque, M. (2011). A large maize (*Zea mays* L.) SNP genotyping array: Development and germplasm genotyping, and genetic mapping to compare with the B73 reference genome. *PLoS One*, *6*, 15.

Gholipoor, M., Choudhary, S., Sinclair, T. R., Messina, C. D., & Cooper, M. (2013). Transpiration response of maize hybrids to atmospheric vapour pressure deficit. *Journal of Agronomy and Crop Science*, *199*, 155–160.

Gilmour, A. R., Cullis, B. R., & Verbyla, A. P. (1997). Accounting for natural and extraneous variation in the analysis of field experiments. *Journal of Agricultural, Biological, and Environmental Statistics*, *2*, 269–293.

Giraud, H., Lehermeier, C., Bauer, E., Falque, M., Segura, V., Bauland, C., … Moreau, L. (2014). Linkage Disequilibrium with Linkage Analysis of Multi-Line Crosses Reveals Different Multi-Allelic QTL for Hybrid Performance in the Flint and Dent Heterotic Groups of Maize. *Genetics*, *198*, 1717–1734.

Gresset, S., Westermeier, P., Rademacher, S., Ouzunova, M., Presterl, T., Westhoff, P., & Schön, C.-C. (2014). Stable carbon isotope discrimination is under genetic control in the C4 species maize with several genomic regions influencing trait expression. *Plant Physiology*, *164*, 131–143.

Jones, H. G. (1992). *Plants and microclimate: A quantitative approach to environmental plant physiology*. Cambridge, UK: *Cambridge University Press*.

Kholová, J., Hash, C. T., Kumar, P. L., Yadav, R. S., Kočová, M., & Vadez, V. (2010). Terminal drought-tolerant pearl millet [Pennisetum glaucum (L.) R. Br.] have high leaf ABA and limit transpiration at high vapour pressure deficit. *Journal of Experimental Botany*, *61*, 1431–1440.

Kholová, J., Zindy, P., Malayee, S., Baddam, R., Murugesan, T., Kaliamoorthy, S., … Vadez, V. (2016). Component traits of plant water use are modulated by vapour pressure deficit in pearl millet (Pennisetum glaucum (L.) R.Br.). *Functional Plant Biology*, *43*, 423–437.

Koester, R. P., Nohl, B. M., Diers, B. W., & Ainsworth, E. A. (2016). Has photosynthetic capacity increased with 80 years of soybean breeding? An examination of historical soybean cultivars. *Plant, Cell & Environment*, *39*, 1058–1067.

Kozai, T., & Kimura, M. (1977). Direct solar light transmission into multi-span greenhouses. *Agricultural Meteorology*, *18*, 339–349.

Lawson, T., & Blatt, M. R. (2014). Stomatal size, speed, and responsiveness impact on photosynthesis and water use efficiency. *Plant Physiology*, *164*, 1556–1570.

Lawson, T., Kramer, D. M., & Raines, C. A. (2012). Improving yield by exploiting mechanisms underlying natural variation of photosynthesis. *Current Opinion in Biotechnology*, *23*, 215–220.

Lippert, C., Listgarten, J., Liu, Y., Kadie, C. M., Davidson, R. I., & Heckerman, D. (2011). FaST linear mixed models for genome-wide association studies. *Nature Methods*, *8*, 833–835.

Malosetti, M., Ribaut, J.-M., Vargas, M., Crossa, J., & van Eeuwijk, F. A. (2008). A multi-trait multi-environment QTL mixed model with an application to drought and nitrogen stress trials in maize (*Zea mays* L.). *Euphytica*, *161*, 241–257.

Millet, E. J., Welcker, C., Kruijer, W., Negro, S., Coupel-Ledru, A., Nicolas, S. D., … Tardieu, F. (2016). Genome-wide analysis of yield in Europe: Allelic effects vary with drought and heat scenarios. *Plant Physiology*, *172*, 749–764.

Monteith J.L. (1965) Evaporation and environment. Paper presented at the Symp. Soc. Exp. Biol.

Moser, G., Lee, S. H., Hayes, B. J., Goddard, M. E., Wray, N. R., & Visscher, P. M. (2015). Simultaneous discovery, estimation and prediction analysis of complex traits using a Bayesian mixture model. *PLoS Genetics*, *11*. e1004969

Parent, B., Turc, O., Gibon, Y., Stitt, M., & Tardieu, F. (2010). Modelling temperature-compensated physiological rates, based on the co-ordination of responses to temperature of developmental processes. *Journal of Experimental Botany*, *61*, 2057–2069.

Poorter, H., Fiorani, F., Pieruschka, R., Wojciechowski, T., van der Putten, W. H., Kleyer, M., … Postma, J. (2016). Pampered inside, pestered outside? Differences and similarities between plants growing in controlled conditions and in the field. *New Phytologist*, *212*, 838–855.

R Core Team (2014) R: A language and environment for statistical computing. *Vienna, Austria: R Foundation for Statistical Computing*.

Rincent, R., Moreau, L., Monod, H., Kuhn, E., Melchinger, A. E., Malvar, R. A., … Mary-Huard, T. (2014). Recovering power in association mapping panels with variable levels of linkage disequilibrium. *Genetics*, *197*, 375–387.

Rochette, P., Pattey, E., Desjardins, R. L., Dwyer, L. M., Stewart, D. W., & Dubé, P. A. (1991). Estimation of maize (*Zea mays* L.) canopy conductance by scaling up leaf stomatal conductance. *Agricultural and Forest Meteorology*, *54*, 241–261.

Sadok, W., & Sinclair, T. R. (2009). Genetic variability of transpiration response to vapor pressure deficit among soybean (Glycine max [L.] Merr.) genotypes selected from a recombinant inbred line population. *Field Crops Research*, *113*, 156–160.

Shekoofa, A., Sinclair, T. R., Messina, C. D., & Cooper, M. (2016). Variation among maize hybrids in response to high vapor pressure deficit at high temperatures. *Crop Science*, *56*, 392–396.

Sinclair, T. R., Hammer, G. L., & van Oosterom, E. J. (2005). Potential yield and water-use efficiency benefits in sorghum from limited maximum transpiration rate. *Functional Plant Biology*, *32*, 945–952.

Stanhill, G., Fuchs, M., Bakker, J., & Moreshet, S. (1973). The radiation balance of a glasshouse rose crop. *Agricultural Meteorology*, *11*, 385–404.

Stinziano J.R., Morgan P.B., Lynch D.J., Saathoff A.J., McDermitt D.K. & Hanson D.T. (2017) The rapid A–Ci response: Photosynthesis in the phenomic era. *Plant, Cell & Environment*, n/a–n/a

Tanaka, Y., Sano, T., Tamaoki, M., Nakajima, N., Kondo, N., & Hasezawa, S. (2006). Cytokinin and auxin inhibit abscisic acid-induced stomatal

closure by enhancing ethylene production in Arabidopsis. *Journal of Experimental Botany*, *57*, 2259–2266.

Tarara, J. M., & Ham, J. M. (1999). Measuring sensible heat flux in plastic mulch culture with aerodynamic conductance sensors. *Agricultural and Forest Meteorology*, *95*, 1–13.

Tardieu, F., Cabrera-Bosquet, L., Pridmore, T., & Bennett, M. (2017). Plant phenomics, from sensors to knowledge. *Current Biology*, *27*, R770–R783.

Tardieu, F., & Simonneau, T. (1998). Variability among species of stomatal control under fluctuating soil water status and evaporative demand: Modelling isohydric and anisohydric behaviours. *Journal of Experimental Botany*, *49*, 419–432.

Terasaka, K., Blakeslee, J. J., Titapiwatanakun, B., Peer, W. A., Bandyopadhyay, A., Makam, S. N., … Yazaki, K. (2005). PGP4, an ATP binding cassette P-glycoprotein, catalyzes auxin transport in Arabidopsis thaliana roots. *The Plant Cell*, *17*, 2922–2939.

Unterseer, S., Bauer, E., Haberer, G., Seidel, M., Knaak, C., Ouzunova, M., … Schon, C. C. (2014). A powerful tool for genome analysis in maize: Development and evaluation of the high density 600 k SNP genotyping array. *BMC Genomics*, *15*, 15.

Vialet-Chabrand, S. R., Matthews, J. S., McAusland, L., Blatt, M. R., Griffiths, H., & Lawson, T. (2017). Temporal dynamics of stomatal behaviour: Modelling,and implications for photosynthesis and water use. *Plant Physiology*. https://doi.org/10.1104/pp.17.00125

Yang, Z., Sinclair, T. R., Zhu, M., Messina, C. D., Cooper, M., & Hammer, G. L. (2012). Temperature effect on transpiration response of maize plants to vapour pressure deficit. *Environmental and Experimental Botany*, *78*, 157–162.

SUPPORTING INFORMATION

Additional Supporting Information may be found online in the supporting information tab for this article.

How to cite this article: Alvarez Prado S, Cabrera-Bosquet L, Grau A, et al. Phenomics allows identification of genomic regions affecting maize stomatal conductance with conditional effects of water deficit and evaporative demand. *Plant Cell Environ*. 2017;1–13. https://doi.org/10.1111/pce.13083